Spinning Disk Confocal Microscopy of Live, Intraerythrocytic Malarial Parasites. 2. Altered Vacuolar Volume Regulation in Drug Resistant Malaria†

Bojana Gligorijevic,‡ Tyler Bennett,‡ Ryan McAllister,§ Jeffrey S. Urbach,§ and Paul D. Roepe*,‡,||

Department of Chemistry, Department of Biochemistry and Molecular Biology, and Program in Tumor Biology, Lombardi Cancer Center, Department of Physics, and Center for Infectious Diseases, Georgetown University, 37th and O Streets, Washington, D.C. 20057

Received May 24, 2006; Revised Manuscript Received August 1, 2006

ABSTRACT: In the previous paper [Gligorijevic, B., et al. (2006) *Biochemistry 45*, pp 12400-12410], we reported on a customized Nipkow spinning disk confocal microscopy (SDCM) system and its initial application to DIC imaging of hemozoin within live, synchronized, intraerythrocytic *Plasmodium falciparum* malarial parasites. In this paper, we probe the biogenesis as well as the volume and pH regulation of the parasite digestive vacuole (DV), using the fluorescence imaging capabilities of the system. Several previous reports have suggested that mutant PfCRT protein, which causes chloroquine resistance (CQR) in *P. falciparum*, also causes increased acidification of the DV. Since pH and volume regulation are often linked, we wondered whether DV volume differences might be associated with CQR. Using fast acquisition of SDCM *z* stacks for synchronized parasites with OGd internalized into the DV, followed by iterative deconvolution using experimental point spread functions, we quantify the volume of the DV for live, intraerythrocytic HB3 (CQS), Dd2 (CQR via drug selection), GCO3 (CQS), and GCO3/C3^{Dd2} (CQR via transfection with mutant *pfcrt*) malarial parasites as they develop within the human red blood cell. We find that relative to both CQS strains, both CQR strains show significantly increased DV volume as the organelle forms upon entry into the trophozoite stage of development and that this persists until the trophozoite−schizont boundary. A more acidic DV pH is found for CQR parasites as soon as the organelle forms and persists throughout the trophozoite stage. We probe DV volume and pH changes upon ATP depletion, hypo- and hypertonic shock, and rapid withdrawal of perfusate chloride. Taken together, these data suggest that the PfCRT mutations that cause CQR also lead to altered DV volume regulation.

Altered transmembrane ion transport is a hallmark of many examples of drug resistance, particularly for "multi"-drug resistance[1] documented in malaria parasites, cancer cells, and some bacteria. However, the pharmacologic repercussions of these alterations are not fully understood in most cases. Altered ion transport in drug resistant cells was first assessed in the 1970s and was typically rationalized in terms of the physicochemical effects it might exert on passive diffusion of charged, weakly basic, or weakly acidic amphipathic drugs. We now know that altered ion transport in drug resistant tumor cells (e.g., refs *1* and *2*) has multiple effects that have an impact on drug resistance. For example, anticancer drugs kill tumor cells via inducing apoptosis, and it is now well established that apoptosis is regulated by plasma, and mitochondrial, membrane ion transport (*3*, *4*). Thus, ion transport perturbations seen in drug resistant tumor cells influence normal ionic regulation of apoptotic signal transduction and thus have indirect but crucial cytotoxic effects in addition to effects on drug diffusion.

The full range of implications for altered ion transport found in multidrug resistant malarial parasites (e.g., ref *5*) is still being debated. Nonetheless, they are equally provocative since many of the drugs to which these parasites are resistant are diprotic weak bases that act at the digestive vacuole (DV).[2] The DV membrane maintains a high-pH gradient and presumably a high-electrical potential difference dominated by H^+. These provide a large chemical driving force for the passive accumulation of antimalarials such as chloroquine (CQ), and changes in these parameters are predicted to have quite significant effects on drug accumulation. In addition, even subtle alterations of the intra-DV ionic environment regulated by the DV membrane ΔpH and

† Supported by NIH Grants AI56312 and AI45759 to P.D.R. and NSF Grant DBI 0353030 to J.S.U.

* To whom correspondence should be addressed. Telephone: (202) 687-7300. Fax: (202) 687-6209. E-mail: roepep@georgetown.edu.

‡ Department of Chemistry, Department of Biochemistry and Molecular Biology, and Program in Tumor Biology, Lombardi Cancer Center.

§ Department of Physics.

|| Center for Infectious Diseases.

[1] Regardless of the system being examined (e.g., tumor cells, parasites, or bacteria), "multidrug resistance" refers to a spectrum of phenomena for that system that vary widely with regard to the drugs in question, the degree of resistance, and the number and type of genetic events linked to the specific mdr phenotype being examined.

[2] Abbreviations: DV, digestive vacuole; CQ, chloroquine; iRBC, infected red blood cell; Hb, hemoglobin; *d*, diameter; SDCM, spinning disk confocal microscopy; PSF, point spread function; CQR, chloroquine resistance (resistant); CQS, chloroquine sensitive; SCP, single-cell photometry; OGd, Oregon Green coupled to dextran; RBC, red blood cell; NMDG, *N*-methyl-D-glucamine; Hz, hemozoin; PfCRT, *P. falciparum* chloroquine resistance transporter; QN, quinine; MDR, multidrug resistance; MQ, mefloquine; 2D, two-dimensional; 3D, three-dimensional.

10.1021/bi0610348 CCC: $33.50
Published on Web 09/20/2006

membrane potential will have very significant effects on heme chemistry and heme−drug interactions. Heme released from catabolized hemoglobin within the DV is a principle target of CQ and other quinoline-based antimalarials. Heme is likely also a target for xanthone, acridine, acridone, and other pharmacophore-based drugs. Elucidating the ionic environment and ion transport of the DV is central to understanding the molecular pharmacology of heme-targeted antimalarial drugs (*6*−*9*).

Beyond the pharmacologic implications and connections to drug resistance, understanding the regulation of H^+ and other ion transport for the DV is crucial to unraveling the unique cell biology of the intraerythrocytic malarial parasite. As described in recent reviews (e.g., refs *10* and *11*), parasites within the infected red blood cell (iRBC) rapidly metabolize hemoglobin (Hb) to provide room for parasite growth, to adjust the osmotic imbalance, and to provide amino acids for new protein synthesis. Upon proteolysis of Hb, released heme is converted to hemozoin (see refs *9* and *10* and references therein), superoxide is scavenged, and the peptide or amino acid byproducts of Hb digestion are exported from the DV to the parasite cytosol. This biochemistry occurs at a remarkable pace and begins, matures, and ends as the DV rapidly forms, grows, and is then cast aside as the parasite enters schizogony. As described in ref *9*, within a span of approximately 10 h the parasite approaches the apex of a $\sim 10^2$-fold increase in cellular volume that occurs within the iRBC and the DV has formed, grown to full size ($d = 2$ μm), accumulated a full complement of hemoglobinases and other enzymes (*11*), catabolized 1 fmol of Hb, and produced and then detoxified a remarkable amount of toxic free heme from Hb (the net increase in total $[\text{heme}]_{DV}$ is approximately 1 M). Among other remarkable features of this process, organellar osmotic regulation must be particularly robust since a large number of new osmolytes are very rapidly produced. How the parasite DV regulates this osmotic balance is unknown.

Probing the organellar physiology of intracellular parasites is particularly challenging. New tools for imaging DV volume and other aspects of DV physiology are required. We have therefore applied the fluorescence imaging capabilities of a customized SDCM apparatus described in the previous paper (*9*), synchronization of malarial parasite cell culture, and iterative deconvolution procedures using experimentally derived point spread functions (PSF) to rapidly image DV volume for living, moving, intraerythrocytic parasites. We find CQR parasites maintain a larger DV volume than CQS parasites. We compare these volume data to DV pH data obtained via single-cell photometry under similar conditions and observe what appears to be unique pH−volume regulatory coupling for this important organelle.

MATERIALS AND METHODS

Materials

All materials were reagent grade or better and purchased from commercial sources as described in ref *9*. Calibration fluorescent beads (1.0 μm diameter) were purchased from Duke Scientific (Palo Alto, CA), and 0.175 μm fluorescent beads were from Invitrogen (Carlsbad, CA).

Methods

Cell Culture. Routine synchronized merozoite *Plasmodium falciparum* culture and preparation of cells for microscopy (either SDCM or SCP) were conducted as described previously (*5*, *9*), with the following modifications. For DV volume measurements, we incorporated a highly fluorescent probe whose properties were not unduly perturbed by DV pH changes that might accompany some of the experiments (see the Results). For DV pH measurements, we required a ratiometric probe with a pK_a near the value of DV pH. For the latter, we followed methods as described previously (*5*); for the former, we chose to incorporate dextran-conjugated oregon green (OGd).

Krogstad and colleagues previously devised a method for localizing dextran-linked fluorescein to the DV of the intraerythrocytic parasite (*12*). We followed this procedure with some modifications. OGd (Molecular Probes catalog no. D-7170, 488/530 nm, $pK_a = 4.7$) was dissolved in phosphate-buffered saline at a final concentration of 25 mg/mL; 220 μL of a hypotonic solution [5 mM HEPES, 11 mM glucose, and 2 mM MgATP (pH 7.4)] prewarmed to 37 °C was added to 30 μL of the OGd solution. Freshly washed RBCs (100 μL) were slowly added dropwise to this mixture. The suspension was gently mixed for 10 min until an increase in clarity was observed; 250 μL of prewarmed hypertonic solution [280 mM NaCl, 40 mM KCl, 11 mM glucose, and 2 mM MgATP (pH 7.4)] was then added to reseal the permeabilized OGd-loaded RBCs. ATP was included to assist merozoite invasion of resealed RBC ghosts (*13*). The suspension was lightly shaken and centrifuged for 5 min at 2500 rpm in a Beckman clinical centrifuge. The supernatant was removed, and 10 mL of incomplete medium was added. The cells were gently mixed and centrifuged, and the medium wash was then repeated once more. Hemolysis during this procedure induces loss of ~20% of the cells; the 80 μL of packed RBCs remaining were divided equally and added to two flasks each containing 10 μL of either synchronized CQR or CQS parasites at trophozoite stage and at 4% parasitemia, and an additional 5 mL of culture medium was immediately added.

If hypotonic loading is too harsh, merozoites will not invade the OGd-loaded red cells with high efficiency. On the other hand, more gentle hypotonic conditions ensure a number of nonlysed RBCs (15−30% vs 85−70% OGd-loaded) in the final suspension. To allow one cell cycle through unlabeled RBCs (such that a uniformly high number of parasites are then growing within only labeled RBCs), the cells were used in microscopy experiments 60−90 h after addition of loaded RBCs to the 4% parasitemia cultures (see the Results).

ATP Depletion, Osmotic Shock, and Cl^- Substitution. We have previously described in detail our procedures for single-cell photometry (SCP) performed under continuous perfusion (*5*). We used these perfusion methods for both SCP and SDCM experiments described in this paper. Such an approach allows us to alter cell perfusate quickly and uniformly while monitoring subcellular pH, volume, etc., in real time. For ATP depletion experiments, normal CO_2/HCO_3^- balanced perfusate containing 5 mM glucose was exchanged for perfusate with 2-deoxyglucose in place of glucose. For Cl^- substitution experiments, Cl^- in the normal perfusate

was rapidly replaced with an equimolar amount of glutamate or gluconate (in general, except where noted, the two replacement anions provided similar results). For hypo- or hypertonic shock experiments, we first selectively permeabilized the RBC and parasite plasma membrane via careful saponin titration as described in the Results to provide rapid osmolyte access to the DV membrane. Perfusate was then switched to 150 or 600 mOsm/kg (0.5- or 2.0-fold osmolality, respectively) to induce DV swelling or shrinkage. Distilled water or decreased NaCl content was used in the former, and additional 150 mM NaCl or NMDG (*N*-methyl-D-glucamine) was used in the latter.

Single-Cell Photometry (SCP) and Spinning Disk Confocal Microscopy (SDCM). SCP was as described in detail previously (*5*, *14*) using custom systems comprised of a Nikon diaphot microscope, a Photometrics Sensys 12-bit CCD camera, associated optics, custom perfusion cells, and custom dynamic thresholding software.

Fluorescence Mode SDCM. (1) Data Acquisition. We began fluorescence experiments similar to DIC experiments described in the previous paper. Transmittance was focused until Hz within the living parasite DV was clearly visible and presented the largest diameter possible, which defined the *z* axis position as "0". We then switched to fluorescence imaging and acquired a series of images in successive 0.20 μm *z* axis displacements. The fluorescence of entrapped probes was excited with a mixed gas laser; excitation was typically at 488 nm. The average laser power measured from the objective was 260 μW, and exposure times were 100 ms, giving 417 μmol of photons s^{-1} m^{-2}. The field of view was limited to $\leq$25% (center quarter) of maximal to reduce collection time, and 16-bit tiff image stacks were exported to a portable hard drive.

(2) Deconvolution. Diffraction and spherical abberation result in degradation of acquired cell fluorescence images (*15*). In principle, deconvolution reverses optical "convolution" and is based on a mathematical or empirical estimation of the behavior of a point light source called the point spread function (PSF). To measure the appropriate PSF, we collected light along all three axes (*x*, *y*, and *z*) from small fluorescing beads (subdiffraction limit) embedded in a variety of media, including hydrated red cells, and using the same microscope parameters that were used in collection of data from live parasites.

Deconvolution was performed with the iterative maximum likelihood estimation (MLE) algorithm adapted by AutoQuant (*16*, *17*) which allows either a theoretically calculated (*18*) or experimentally obtained PSF. To obtain experimental PSFs, we mixed subresolution ($d \leq 0.17$ μm) fluorescent beads (Molecular Probes catalog no. P 7220, 505/515 nm) in cell culture and then imaged under the same conditions that were used for data collection for parasites. These beads also had excitation and emission wavelengths similar to those of OGd. As in our DIC approach (*9*), improvements in the quality of the deconvolution were monitored by measuring the dimensions and calculated volume of a 1 μm polystyrene bead (Duke Scientific catalog no. G0100, 468/508 nm).

(3) 3D Restoration, Segmentation, and DV Volume Measurements. Restoration and volume measurements were conducted using the Imaris 4.2.0 software package from Bitplane run on a Dell mini tower customized with three 750 Gb RAID hard drives and 8 Gb RAM. After the SDCM *z* series of optical sections ("*z* stacks") acquired from fluorescent DV had been imported into Imaris, the data were first deconvolved using the AutoQuant X module as described above. The imported PSF obtained under the same imaging conditions was used to initialize the deconvolution routine, and data sets were deconvolved using $\geq$15 iterations (*19*, *20*). The deconvolved stack was then imported back into the 3D-rendering module of Imaris and assembled. After the average background intensity had been subtracted, the full range of intensities was normalized to account for small differences (<5%) in emission for different cells. To measure the volume of the vacuole, an isosurface of the restored data set at half-peak intensity was built in Imaris, and its characteristics were then exported into Excel, where the values for >20 cells per sample were averaged and expressed as cubic micrometers per cell $\pm$ the standard deviation.

In the volume versus time experiments, time point normalization add-on was used to account for minor bleaching. This Matlab routine normalizes the voxel intensities for each time point of a four-dimensional data set.

RESULTS

Figure 1 illustrates our methodology for measuring DV volume and pH versus maturation of the malarial parasite within the infected human red blood cell. After invasion of red cells to form the ring stage, *P. falciparum* malarial parasites enter the "feeding" (trophozoite) stage within 14−15 h. Over the ensuing 15 h, the parasite DV forms, matures, and catalyzes the rapid degradation of approximately 85% of red cell hemoglobin (*9*). If red cells are incubated with a dextran-conjugated fluorophore under mild hypotonic conditions, followed by resealing with hypertonic solution (Figure 1A, steps 1 and 2), the dextran−fluorophore conjugate is trapped within the red cell (Figure 1B, top left). Following infection of the preloaded red cells (Figure 1A, step 3), parasites concentrate the fluorophore within the DV as the DV develops (Figure 1B). As the DV grows, fluorescence is both progressively lost from the red cell cytosol and concentrated within the DV (Figure 1B); thus, net DV fluorescence is always higher than that of the red cell, regardless of the stage of DV maturation. Once the DV is labeled, vital dye characteristics can be monitored via photometry to analyze pH and other physiologic parameters (e.g., ref *5*). Also, even though the parasites rapidly wiggle within the iRBC, the 3D morphology of the living DV can be analyzed via SDCM (Figure 1A, steps 4−7), because SDCM can generate full *z* stacks in <1 s (*9*).

Using the fluorescence capabilities of the novel SDCM apparatus described in Methods and ref *9*, as well as highly synchronized parasite culture (*9*), we acquired high-resolution *z* stacks of fluorescent DV versus time of parasite maturation within the iRBC. Similar to DIC data discussed in ref *9*, the *z* stacks were assembled within Imaris. They were then iteratively deconvolved using Autoquant software and experimental point spread functions (PSF), and voxel counting was done to quantify volume (see Methods). Figure 2 shows raw data (top) and deconvolved data (bottom) for a 1.00 μm diameter fluorescent bead (left, A and B) and for a DV from a living parasite within the iRBC under constant perfusion (right, C and D). Data are shown in the $x-y$ (A−D) and $x-z$ (A′−D′) orientations. As expected, blurring is greater

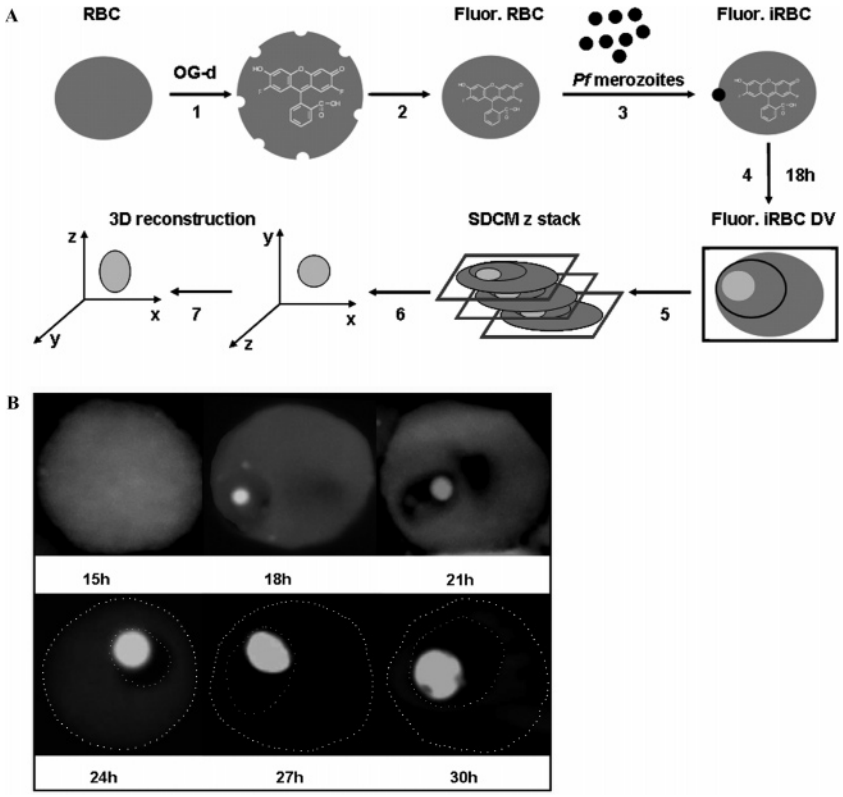

FIGURE 1: (A) DV fluorescence loading and imaging procedure. RBCs were washed, and mild hypotonic shock was performed in the presence of OGd (1) followed by resealing with hypertonic wash (2), infection with *P. falciparum* (3), and maturation of the iRBC for different times, with concomitant development of the DV within the parasite (4). Fluorescent DV *z* stacks were then obtained via SDCM (5) as described (see Methods), rendered into 3D data sets using Imaris (6), and iteratively deconvolved and analyzed by voxel analysis (7). (B) Progressive concentration of OGd within the DV shown in single *z* slices of SDCM *z* stacks, obtained at different times postinvasion, reveals DV biogenesis. In the second cycle after the introduction of the dye into the RBCs, a synchronized Dd2 culture was sampled every 3 h during the cell cycle. The stage of the parasites was verified visually via DIC. As fluorescence within the RBC cytosol was lost, we outlined the iRBC plasma membrane and parasite plasma membrane with dotted white lines (bottom, 24−30 h). Note also the apparent lack of significant fluorescence within the parasite cytosol, while high fluorescence is seen in RBC cytosol and the DV (top right, 21 h), suggesting direct traffic between the DV and the RBC cytosol. Images were obtained using 488 nm excitation, a 510LP filter, an exposure time of 100 ms, 50% laser power, 0 gain, and a 100× oil NA 1.4 objective.

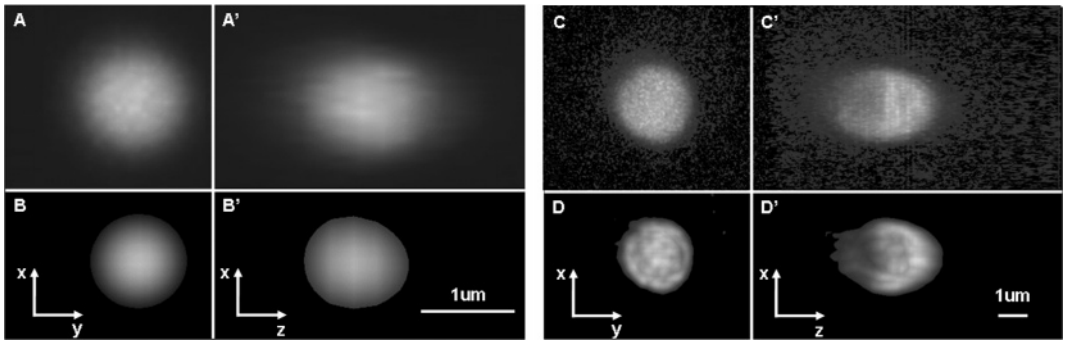

FIGURE 2: Example of raw (A, A′, C, and C′) and iteratively deconvolved (B, B′, D, and D′) SDCM data for one *z* slice in the *x*−*y* (A−D) and *x*−*z* (A′−D′) orientations. Data on the left are for a 1.00 μm *d* fluorescent bead, and data on the right are for a late stage trophozite DV (see the text).

in the axial (*x*−*z*) direction than in the lateral (*x*−*y*) direction (cf. panels A′ and C′ of Figure 2 vs panels A and C), but upon iterative deconvolution using experimental PSF, the *x*−*z* diameter was within 5% of known values for fluorescent beads of various diameters (0.5−2.5 μm, data not shown). The deconvolved *x*−*y* diameter was within 1% for these beads. Note DV volumes are calculated via explicit voxel counting, not via any geometrical formula dependent on the *x*−*y* or *x*−*z* diameter.

Figure 3 shows representative 2D projections of late stage trophozoite DV for CQR strains Dd2 (top left) and C3Dd2 (bottom left) and CQS strains HB3 (top right) and GC03 (bottom right). In each case, the *z* slice harboring the largest DV cross-sectional area for the imaged cell is shown. On the left-hand side in each panel are the raw data after thresholding (see Methods), and on the right-hand side are the iteratively deconvolved (see Methods) data. Even though the DVs are conspicuously nonspherical, from initial perusal of such projections it appeared to us that the DV for CQR strains had a larger cross-sectional area than the DV for CQS strains. However, due to the irregular shape, and because *x*−*y* versus *x*−*z* dimensions are not defined for the DV in

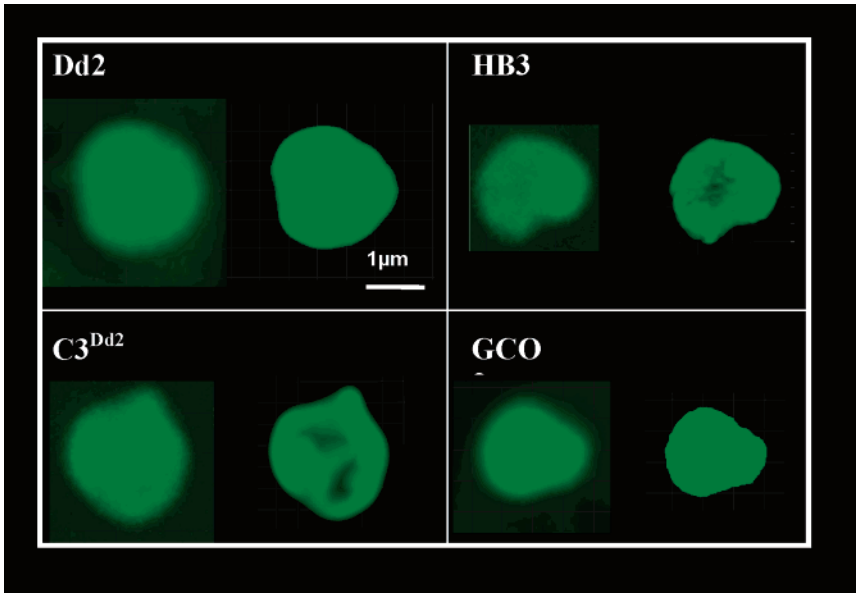

FIGURE 3: Representative 2D projections of OGd-loaded DV for synchronized parasite cultures (CQR strains Dd2 and C3Dd2, left; CQS strains HB3 and GCO3, right). In each panel, the raw projection after thresholding is shown, followed by the iteratively deconvolved image. See Methods for imaging conditions and data processing parameters.

an absolute sense, it is impossible to use such data to precisely quantify any differences in DV size.

Thus, we avoided the temptation to process cross-sectional areas and instead collected full SDCM *z* stacks to quantify DV volumes via voxel analysis. Panels A and B of Figure 4 plot the kinetics of DV biogenesis for CQS (empty symbols) and CQR (filled symbols) malarial parasites [HB3 vs Dd2 (Figure 4A) and GCO3 vs $C3^{Dd2}$ (Figure 4B)]. Notably, CQR parasites clearly develop a significantly larger DV than CQS do as CQR parasites mature within the iRBC. This effect is due to the presence of the mutated PfCRT protein in the DV membrane and not epiphenomena caused by antimalarial drug exposure in the laboratory, since mutant *pfcrt* transfectants ($C3^{Dd2}$, Figure 4B) exhibit a similarly increased DV volume versus time relative to laboratory CQR strain Dd2.

This result is perhaps not surprising since previously we measured a more acidic pH for the DV of CQR parasites relative to CQS controls (*5*). However, these pH measurements were made only at a single point in organellar biogenesis corresponding to the late trophozoite stage (25−28 h). There has been disagreement in the literature regarding the magnitude of this DV acidification, so we wondered if the acidification might be stage-dependent (e.g., dependent upon the degree of DV maturation and the relative difference in CQS vs CQR DV volumes). Figure 5 plots DV pH versus time of iRBC maturation for CQS (empty bars) versus CQR (filled bars) parasites. Again, we compare lab strains Dd2 and HB3 (Figure 5A) and the transfectant model strains $C3^{Dd2}$ and GCO3 (Figure 5B). Interestingly, a more acidic DV pH is measured for both CQR strains as soon as the DV develops and persists throughout maturation of the organelle. Importantly, these measurements are made one cell at a time for intact iRBC, via single-cell photometry (SCP) under continuous physiologic perfusion with CO_2/HCO^-_3 balanced perfusate, not via depositing 10^5-10^6 detergent-extracted parasites into bulk (nonperfused), artificially buffered solutions within a fluorometer cuvette as in another recent study (e.g., ref *21*). As might be expected since pH and volume regulation are typically mechanistically coupled, via these SDCM and SCP data, CQR parasites exhibit both a larger steady state DV volume and a lower steady state DV pH. Moreover, these effects are apparently due to CQR-associated mutations in the PfCRT protein (Figures 4B and 5B and ref *5*). One obvious possibility is that increased H^+ activity within the DV promotes DV accumulation of a counteranion(s), leading to DV swelling. Alternatively, normal DV osmolyte traffic is disrupted in CQR parasites. Regardless, mutant PfCRT mediates this altered ion (and/or osmolyte) traffic, directly or indirectly.

To probe the basis of perturbed volume and pH regulation for the CQR DV, we first tested whether our methodology reliably reported expected regulatory processes, including those seen previously for other lysosomes (the DV is ostensibly a specialized lysosome optimized for Hb digestion and FPIX processing). For example, we depleted parasite ATP by replacing glucose in the perfusate flowing over the cells with 2-deoxyglucose (first upward-pointing arrow in Figure 6A,B). Intraerythrocytic *P. falciparum* produce ATP via anaerobic metabolism, and the DV membrane harbors a H^+-ATPase that generates the high-DV membrane pH gradient. ATP depletion is expected to inhibit the DV H^+-ATPase and should rapidly collapse the DV pH gradient. Not surprisingly, this is indeed the case (Figure 6A,B). The collapse of the DV pH gradient we measure under continuous perfusion via SCP is more rapid than that measured previously using bulk parasite culture deposited into a fluorometer cuvette without perfusion (*21*). This may be due in part to more efficient ATP depletion under perfusion versus bulk solution conditions. We note that the rate of collapse for CQS versus CQR parasites is similar but not identical (compare panels A and B of Figure 6, 200−400 s). Also, despite beginning at a different steady state DV pH [CQR parasites exhibit a lower initial DV pH as reported previously (*5*)], in both cases DV pH collapses to near the cytosolic pH values measured previously for the two strains [frequently, but not always, CQR parasites exhibit more alkaline cytosol (e.g., ref *22*)]. To assess this complete collapse of DV pH, unlike previous work with bulk culture in a cuvette (*21*), we used

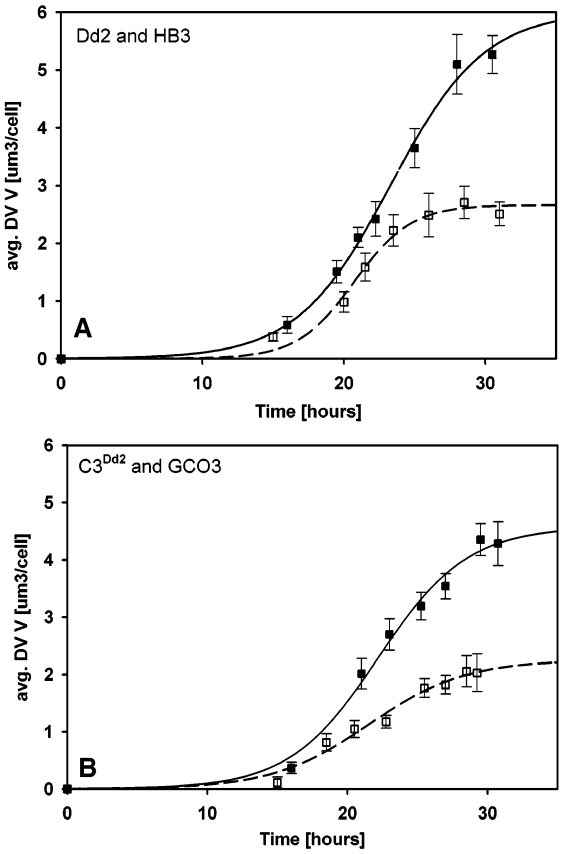

FIGURE 4: Biogenesis of the digestive vacuole for (A) Dd2 [CQR (■)] and HB3 [CQS (□)] laboratory strains and for (B) $C3^{Dd2}$ [CQR (■)] and GCO3 [CQS (□)] model transfectant strains (strain C3 has been transfected with the CQR-associated PfCRT "Dd2" allele). RBCs were labeled with OGd and infected with tightly synchronized late trophozoites (Figure 1). After the cells had entered the second cycle, the fluorescent DV were imaged in 3D by SDCM. Each time point represents an average (±standard deviation) of DV volume (DV *V*) measured for >20 individual digestive vacuoles. Images were obtained using 488 nm excitation, a 510LP filter, an exposure time of 100 ms, a 50% laser power, 0 gain, a 100× oil NA 1.4 objective, and 0.20 μm *z* spacing. DV images were deconvolved using batch deconvolution within the AutoQuant iterative 3D deblur algorithm (contains MLE/CI) with 20 iterations and in fixed PSF mode. A 175 nm fluorescent bead imaged under the same conditions was used as the PSF.

multiple SCP samples harboring ratiometric pH indicators with different pK_a values within the DV, performed multiple experiments in parallel, and calibrated both probes for individual cells in situ and under continuous perfusion over a range of pHs (second, third, fourth, and fifth downward-pointing arrows, Figure 6A,B caption). We reasoned this would be necessary because of the large magnitude of the pH gradient. Indeed, the first probe that was utilized (DM-NERF) provides data (light gray lines; 0−400 and 750−1200 s) that is of course unresolvable well above its pK_a (5.4), whereas the second (BCECF, dark lines; 400−750 and 1200−1600 s) does not provide resolvable data well below its pK_a (usable range of 6.5−7.5). Double hash marks in panels A and B of Figure 6 indicate where the two data sets are merged together. When shown together (Figure 6A,B), composite data from the two parallel experiments reveal the full range and true kinetics of the expected DV pH gradient collapse. One probe alone is clearly insufficient. Note also that the steady state DV pH measured via SCP under continuous perfusion (from 0 to 180 s, Figure 6A,B) is not

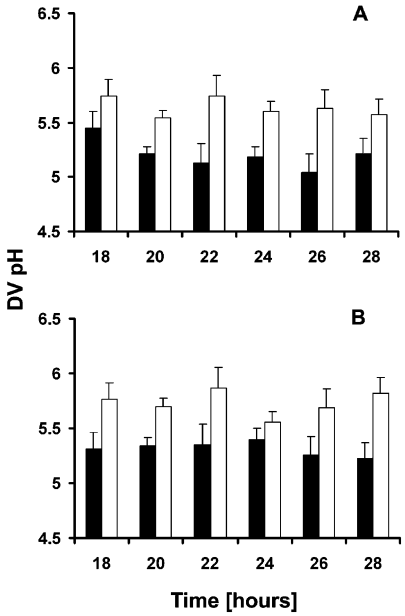

FIGURE 5: Steady state DV pH measured as in ref *5* for CQR (black bars) and CQS (white bars) parasites at different times after infection [(A) Dd2 vs HB3 and (B) C3Dd2 vs GC03 as in Figure 3].

merely equal to the pK_a of the incorporated probe which had been claimed previously from data obtained in bulk cuvette experiments without perfusion (*21*). As pointed out previously (*5*), if $[probe]_{DV}$ is below the measured buffering capacity, when the complexities inherent to bulk solution fluorescence measurements are eliminated via low excitation and thin layer SCP fluorescence measurements, and when cells are continuously perfused with physiologic perfusate harboring proper CO_2 tension, then physiologic DV pH is measured.

Figure 6C shows the DV volume changes that occur upon ATP depletion for CQS (empty symbols) and CQR (filled symbols) parasites. Interestingly, the DV volume increases significantly for CQS parasites upon ATP depletion, but CQR parasites exhibit a much less pronounced increase (nearly 4-fold smaller). This may be because the CQR parasite DV is already swollen under basal conditions (cf. Figure 4) such that there is an intrinsically reduced ability of the CQR DV to swell further, or it may indicate altered osmolyte traffic in response to DV pH collapse. Regardless, we note the volume increase is constant for >30 min (data not shown), indicating the lack of a regulatory volume decrease (RVD) response for the DV under these conditions.

We next reversed the order of pH and volume changes. DV pH collapse promoted by ATP starvation appears to be linked to a volume change (Figure 6), so we probed whether volume changes altered the pH in a symmetrical fashion, which occurs for the cytosol of some eukaryotic cells. To rapidly generate DV volume changes in either direction and then inspect whether reciprocal DV pH changes occurred, we wished to expose the DV to simple hypo- or hyperosmotic shock. Unfortunately, since three other membranes lie between the perfusate and the DV membrane (RBC plasma membrane, parasite parasitophorous, and plasma membranes), inducing rapid volume changes by a conventional rapid change in perfusate osmolality is impossible with standard methods. However, by carefully titrating saponin in the perfusate (Figure 7), we were able to identify

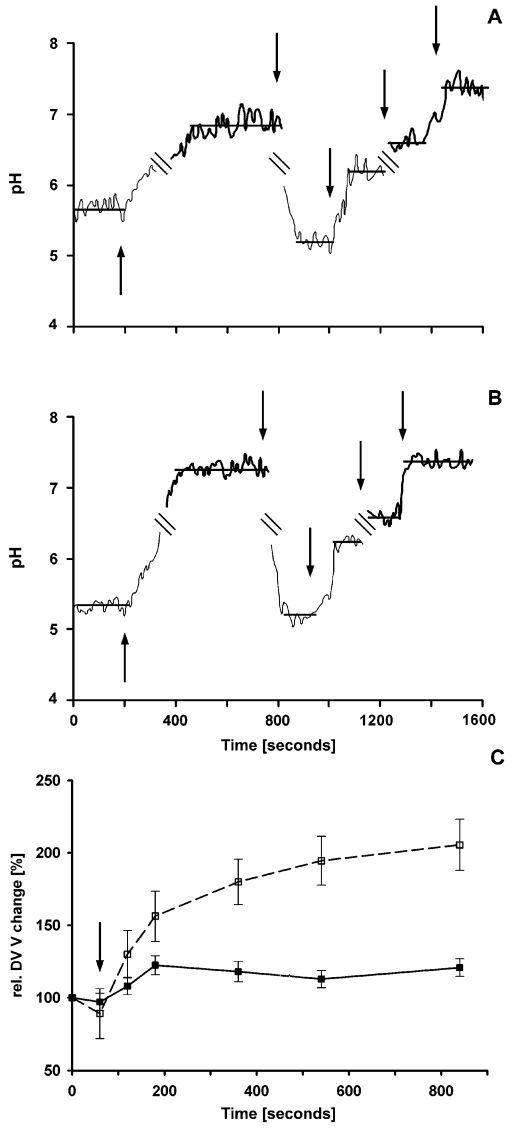

FIGURE 6: Collapse of DV pH for (A) CQS HB3 and (B) CQR Dd2 parasites upon changing normal perfusate flowing over the iRBC to perfusate with 2 mM 2-deoxyglucose in place of glucose (first upward-pointing arrow). Note the more rapid increase in DV pH (from a lower initial pH) for the CQR parasites and collapse to cytosolic pH previously measured for these parasites (*22*). Hash marks indicate where data using NERF fluorophore (light lines) and BCECF fluorophore (dark lines) from parallel experiments were integrated (see the text). At the downward-pointing arrows, perfusate was changed to calibration solution harboring protonophores at pH 5.20, 6.20, 6.60, and 7.40. Straight line fits to the data between the arrows (as shown) were used to average individual points and extrapolate physiologic pH (0−800 s) from the in situ calibration points (see ref *5* and references therein). Each trace represents the average of more than six individual parasites recorded one cell at a time (see ref *5*). In panel C, we show DV volume measured under similar conditions for the same parasites [CQS (□) and CQR (■)]. The downward-pointing arrow denotes glucose substitution. Each point is the average of at least 20 parasites (±standard deviation).

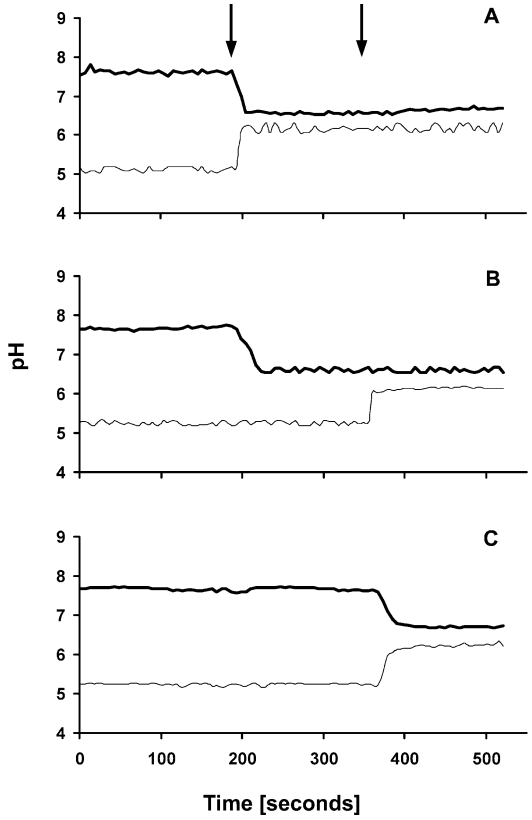

FIGURE 7: Illustration of the saponin titration strategy for DV access: (A−C) 0.07, 0.05, and 0.03% saponin treatment, respectively. The top (thick) line is the cytosolic pH measured with BCECF, and the bottom (thin) line is DV pH measured with NERF. The first downward-pointing arrow indicates changing perfusate from normal to perfusate at pH 6.60 (for BCECF experiments) or 6.20 (for NERF experiments) without any protonophore, and the second arrow denotes addition of the protonophore; 0.05% treatment selectively permeabilizes RBCs and parasite PM, without permeabilizing the DV membrane (see the text). Fluorescent images of parasites exposed to different saponin concentrations will be published elsewhere (T. N. Bennett, M. Ferdig, and P. D. Roepe, submitted for publication).

conditions under which the RBC and parasite plasma membranes were permeant to H^+, but under which the DV membrane was not (Figure 7B). This is evidenced by a fast change in parasite cytosolic pH with a change in the pH of the perfusate in the absence of an ionophore (Figure 7B, top trace, first arrow at 180 s) but a constant DV pH until the ionophore is added (bottom trace, second arrow, Figure 7B). Below this level of saponin treatment, neither membrane was permeant to H^+ in the absence of ionophore (Figure 7C), and above this level, both membranes were similarly permeant (Figure 7A), since both cytosolic and DV pH rapidly converged to perfusate pH.

Figure 8A−C shows changes in DV volume measured by SDCM upon hypertonic (A,B) or hypotonic (C) shock using the saponin titration strategy, and Figure 8D−F shows the concomitant pH changes measured via SCP under similar perfusion conditions in parallel experiments. Notably, hypertonic shock with either NMDG-Cl (Figure 8A) or NaCl (Figure 8B) produced rapid DV shrinkage as predicted. The kinetics and magnitude of DV shrinkage were found to be similar for CQS (empty symbols) and CQR (filled symbols) parasites when NaCl was used (Figure 8B), but when NMDG-Cl was used, DV shrinkage was considerably larger for CQS parasites than for CQR parasites. Also, shrinkage in CQS parasites is greater upon NMDG-Cl shock versus hypertonic NaCl. This is expected, since the CQS DV membrane is likely more permeant to NaCl than NMDG-Cl. These data again suggest different osmolyte permeabilities for the CQR and CQS parasite DV membrane. In contrast, hypotonic shock produced similar swelling in the two parasite strains (Figure 8C), suggesting altered osmolyte

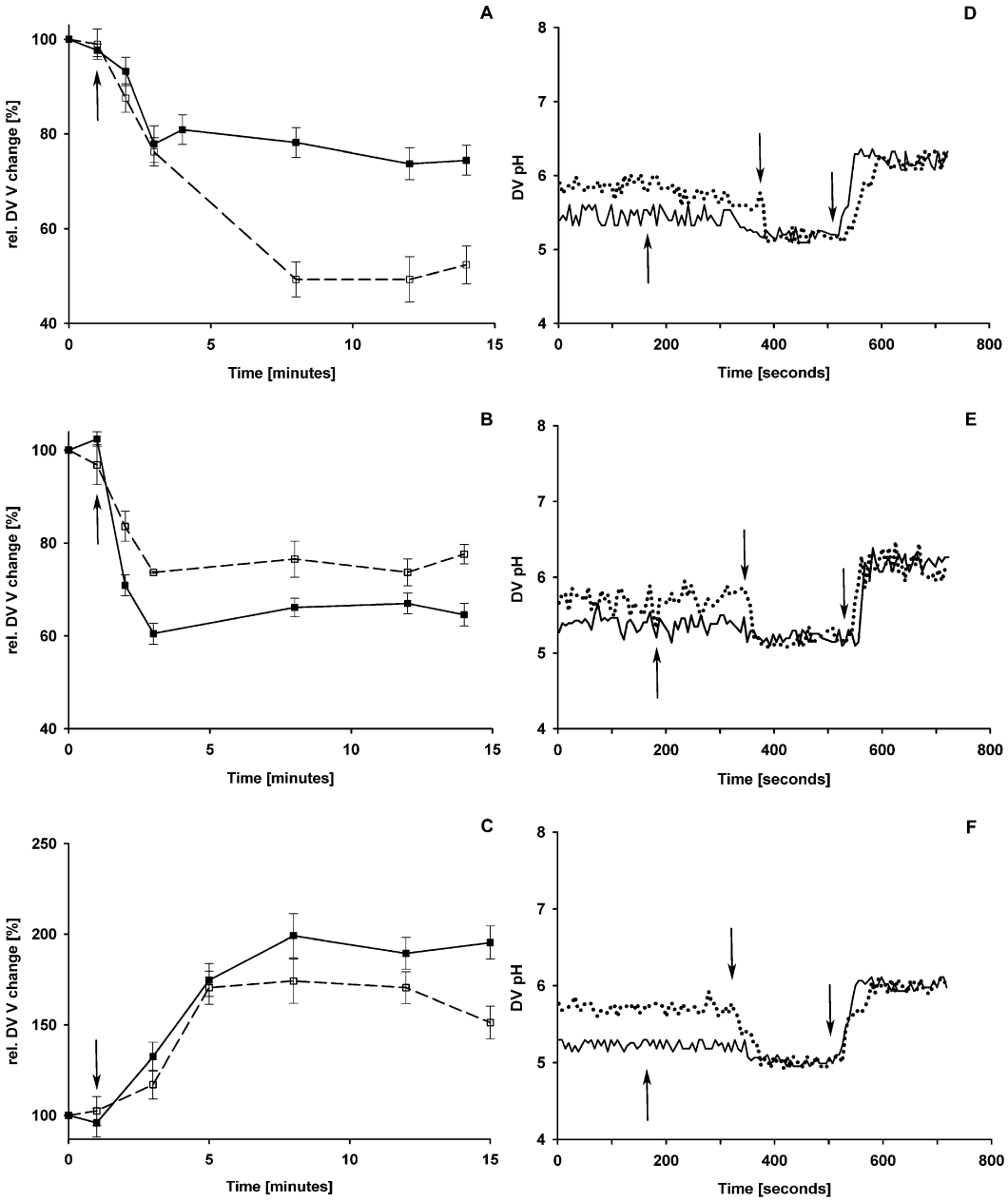

FIGURE 8: DV volume (A−C) and pH (D−F) data for CQR (■) and CQS (□) parasites. Panels A, B, D, and E depict hypertonic shock (600 mOsm at the arrow) using either NMDG-Cl (A and D) or NaCl (B and E) as the additional osmolyte. Panels C and F depict hypotonic shock (150 mOsm). Each point is the average of at least 20 parasites (±standard deviation).

traffic for CQR DV may have a directional bias. Interestingly, neither CQS nor CQR parasites exhibited any DV pH change upon hyper- or hypotonic shock (Figure 8D−F), showing that under these conditions, DV volume and pH regulation are uncoupled, which means that osmolyte traffic in response to osmotic stress is not strictly coupled to transport of acid or base.

Since one model that has been offered to explain how DV pH is lowered in CQR parasites is that mutant PfCRT might confer altered Cl^- permeability in some fashion (*23*), we next tested whether rapid Cl^- substitution had any significant effect on DV pH or volume and whether any such effects differed for CQR versus CQS parasites. Figures 9 and 10 show DV volume and pH transients upon isotonic substitution of Cl^- with gluconate, followed by recovery upon replacement of perfusate Cl^-, again using the saponin titration "rapid ion access" approach described above so that the perturbations in ion concentration were virtually instantaneous. As expected, loss of DV Cl^- promoted by substitution of perfusate Cl^- with gluconate promotes DV shrinkage, presumably upon compensatory movement of a countercation and water (first arrow, Figure 9A,C). Both CQS and CQR parasites exhibit similar DV shrinkage and similar, nearly symmetrical, recovery upon return of Cl^- to the perfusate (second arrow, panel A vs panel C of Figure 9). Similar Cl^- substitution monitored by SCP either in the presence or in the absence of proper CO_2/HCO_3^- does not reveal any change in DV pH for either CQS or CQR parasites (Figure 10A).

Since the PfCRT protein in CQR and CQS parasites has been shown to bind the antimalarial drug CQ (*24*) but since CQR and CQS parasites have different IC_{50} values for CQ, we tested whether the presence of CQ affected the volume change produced by rapid Cl^- substitution. Quite interest-

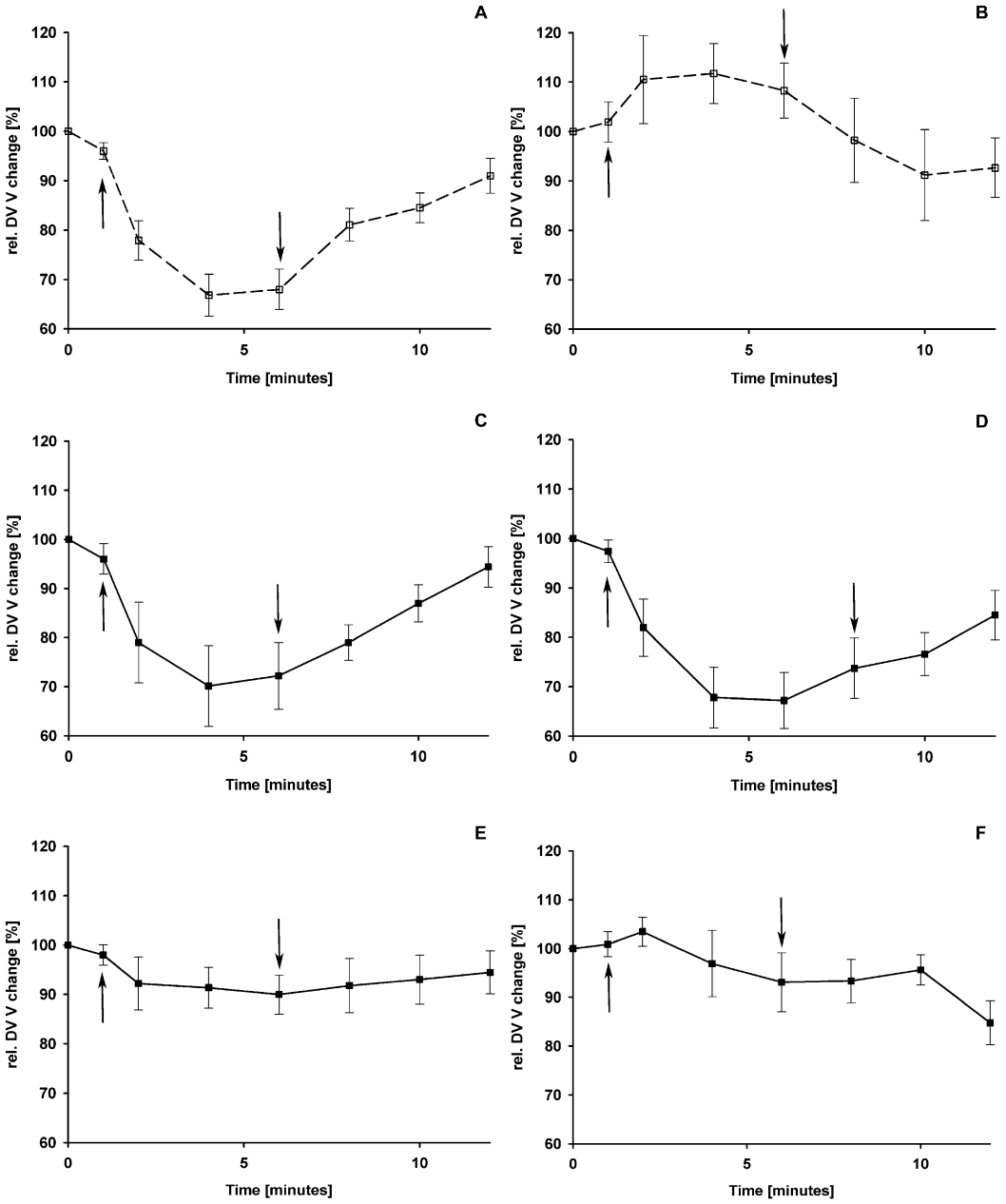

FIGURE 9: DV volume changes upon isotonic Cl^- substitution in the perfusate (equimolar gluconate as the replacement anion). Empty squares depict data for CQS parasites and filled squares data for CQR. Panels A and C depict data in the absence of CQ and panels B and D data for the case in which 60 nM CQ was added to the perfusate. Panel E depicts data for 600 nM and panel F for 60 nM plus 2 μM VPL. Each point is the average of at least 20 parasites (±standard deviation).

ingly, when CQS parasites were preincubated with a level of CQ equal to $3IC_{50}$ (60 nM), the DV shrinkage produced upon Cl^- withdrawal was completely blocked (Figure 9B). Smaller doses showed a dose-dependent intermediate effect (data not shown). Even more interestingly, at a similar absolute dose of CQ, CQR parasite DV shrinkage was not blocked (Figure 9D) but was instead similar to that with Cl^- withdrawal in the absence of drug (compare panel C to panel D of Figure 9). However, importantly, at similar pharmacologic doses (e.g., $3IC_{50}$ for Dd2 = 600 nM), the CQR parasites were completely blocked in Cl^- withdrawal-induced DV shrinkage (Figure 9E), which is similar to the case of CQS DV exposed to 60 nM CQ. Again, intermediate pharmacologic doses showed intermediate effects (not shown). Also, although at 60 nM CQ no effect was seen (Figure 9D), at 60 nM CQ with 2 μM resistance modifier VPL (Figure 9F), CQR DV shrinkage was completely blocked, similar to the effect seen at 600 nM CQ. The presence of IC_{50} levels of CQ did not produce any DV pH change upon Cl^- substitution for either CQS or CQR parasites (Figure 10B,C). Thus, as in the hyper- and hypotonic shock experiments (Figure 8), these data again show that rapid changes in DV pH are uncoupled from rapid volume perturbations.

DISCUSSION

Relatively few studies have quantified vacuolar or lysosomal volume and biogenesis. Even fewer have examined coupling between vacuolar or lysosomal volume and pH. In this study, increased steady state DV volumes versus the stage of maturation is quantified for both laboratory and transfectant model CQR versus CQS malarial parasites. We note that absolute quantification of DV volume can be

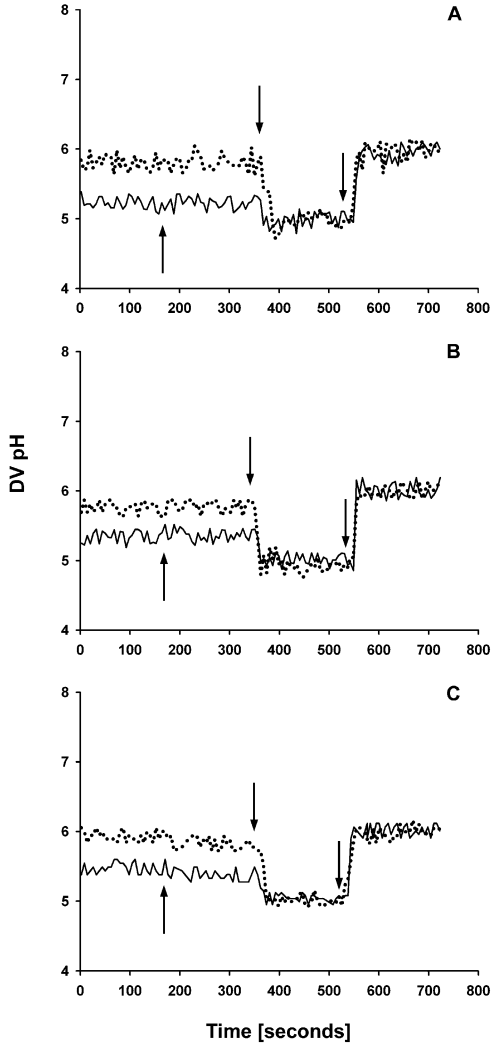

FIGURE 10: DV pH changes measured by SCP upon isotonic Cl^- substitution in the perfusate similar to SDCM experiments shown in Figure 8 (equimolar gluconate as the replacement anion). Dotted lines depict data for CQS parasites and solid lines that for CQR. The first arrow (upward-pointing) denotes Cl^- substitution, whereas the second and third arrows denote changing the perfusate to calibration solution (pH 5.0 and 6.0) and protonophore. Panel A is in the absence of CQ, panel B in the presence of 20 nM CQ, and panel C in the presence of 600 nM CQ in the perfusate. These data were obtained in the presence of proper CO_2 and HCO_3^-; nearly identical data (except for the value of initial DV pH) were obtained in their absence (not shown). Each trace represents the average of more than six individual parasites recorded one cell at a time (see ref *5*).

influenced slightly by the shape and orientation of the DV within the iRBC but that the differences in volume reported here for CQR versus CQS DV are very well above our limits of detection. We conclude that increased DV volume is an important characteristic of the CQR *P. falciparum* phenotype and that it is caused by PfCRT mutations known to cause CQR. This is not entirely surprising since PfCRT is localized to the DV membrane (*25*), CQR-associated PfCRT mutations also cause DV pH perturbations (*5*), and compartmental pH and volume perturbations are often linked. We also find that the DV pH is more acidic for CQR than for CQS parasites at all stages of DV biogenesis that we can measure and that DV volume is similarly but progressively larger for CQR versus CQS at all stages. There are a variety of important pharmacologic and cell biological/biophysical implications.

For example, these initial observations led us to suspect that DV volume and pH regulation might be tightly coupled via ion transport across the DV membrane, as is the case across many eukaryotic plasma membranes, meaning significant perturbations in one parameter would induce perturbations in the other, in symmetrical fashion. Such coupled volume and pH regulation is typically due (in part) to ion exchangers that regulate stoichiometric exchange of acid or base with important osmolytes. However, although a DV volume increase is indeed coupled to rapid loss of the DV pH gradient upon ATP depletion, we find that fast pH changes are not coupled to rapid DV volume perturbations in either direction (i.e., rapid hyper- or hypotonic shock). One immediate conclusion is that certain conventional, well-characterized ion exchange processes are unlikely to be dominant players in DV pH and volume control.

Due to the massive rate of Hb catabolism in the DV, osmolyte production and osmotic balance for the DV is profound and unusual. The full array of Hb byproducts produced with the DV are not known. Short peptides are produced (*11*), but whether free amino acids are also produced is not known. Regardless, the osmolyte traffic necessary for DV volume control must be somewhat unique. Moreover, unlike lysosomes of higher eukaryotes that can exhibit a pH of $\leq$4.5, the DV pH is relatively high for a lysosome-like organelle (*5*). Thus, some degree of unusual volume−pH coupling for the DV is perhaps not surprising.

Cytosolic pH and volume regulation are tightly coupled for many cells since key, ubiquitous pH regulators (e.g., Na^+/H^+ and Cl^-/HCO_3^- exchangers) exchange important osmolytes (i.e., salt ions) for acid or base. However, this coupling concept has not been as extensively explored for vacuoles or lysosomes, where the presence of Cl^- channels and Cl^-/H^+ exchange processes can create very different bioenergetic scenarios. Using a ratio imaging method, one recent study measured acidification coupled to a significant volume increase under steady state conditions for Chinese hamster ovary endosomes (*26*). Lang and colleagues (*27*) have indirectly probed the relationship between pH and volume for astroglial cell lysosomes by perturbing cytosolic swelling via osmotic stress and found that the decrease in steady state lysosomal volume predicted to accompany these perturbations generated a nearly 1 unit alkalinization of steady state lysosomal pH. This is essentially the mirror image of the volume−pH relationship found in the CHO endosome study (*26*); that is, if increased steady state organellar volume is associated with acidification, decreasing the volume might be expected to instigate the opposite. In the study presented here, increased steady state volume for the CQR DV is associated with a lower DV pH, similar to the trend found in refs *26* and *27*. Similarly, cultured plant cells exhibited an increased steady state vacuolar volume upon hypertonic stress that was accompanied by stimulated vacuolar ATPase activity consistent with vacuolar acidification (*28*). Increased organellar volume accompanied by acidification was also recently seen for chromaffin cell secretory vesicles by Sulzer and colleagues (*29*). Thus, the extents of the steady state DV volume and pH perturbations we measure during iRBC development of CQR versus CQS malarial parasites are in general consistent with the few examples recently published for other lysosomal or vacuolar-like organelles.

However, from analysis of genome data, it is also true that malarial parasite membrane bioenergetics appears to involve a blend of transport processes found in animal, plant, and fungal cells. Since in all the examples cited above steady state vacuolar volume (increase or decrease) follows the internal activity of H^+, our initial expectation was that tight coupling between these parameters would also be found for the DV when we induced very rapid perturbations in volume or pH. Indeed, under rapid ATP depletion conditions, the DV pH increases (H^+ activity decreases) and the DV volume concomitantly increases for HB3 parasites. This is the opposite of the trend seen under steady state conditions (Figures 4 and 5, and above); however, another recent study by Ono et al. also found that rapid ATP depletion increases lysosome size during TNF-induced cell death (*30*). Lysosome pH was not directly measured in this study; regardless, since ATP depletion would reduce the efficiency of H^+ pumping into these lysosomes, these data suggest that a rapid ATP depletion-induced increase in lysosome volume is accompanied by lysosomal alkalinization in this system as well, similar to our observation for the parasite DV.

To our knowledge, direct, rapid perturbation of vacuolar or lysosomal volume by hyper- or hypotonic shock, followed by direct organellar pH measurements, has not previously been attempted, nor has rapid Cl^- withdrawal (to promote rapid loss of vacuolar or lysosomal Cl^-), followed by direct pH measurements. Thus, in this case, to the best of our knowledge, our data are unique and without precedent. It will be important to examine similarities and differences between the behavior of the DV versus other vacuoles or lysosomes, as those data become available. At first glance, the "tight" coupling between DV alkalinization and volume increase upon rapid ATP depletion versus the lack of any apparent pH change upon rapid hyper- or hypotonic shock might appear paradoxical. That is, one set of conditions reveals tight coupling between the parameters (when pH is changed first), whereas the other (when volume is changed first) does not. This behavior therefore suggests that there are likely to be at least two pathways for essential osmolyte transport, that neither is likely to be an acid- or base-coupled ion exchanger, and that these two pathways may have different pH sensitivities.

We further investigated one possible pathway. Earlier work (*5*, *23*) suggested CQR-associated mutant PfCRT might induce altered Cl^- transport properties for the DV membrane. Thus we first examined whether rapid isotonic Cl^- exchange in the perfusate, which will drive the rapid exit of Cl^- from the DV via whichever transport pathway dominates under these conditions, is directly coupled to a DV pH change (since mutation of PfCRT also alters DV pH). Upon Cl^- substitution, a significant DV shrinkage was indeed measured as expected, indicating loss of salt (Cl^- and a countercation). We expected to see a concomitant DV alkalinization as H^+ exited as the requisite countercation, since this has been observed in other settings. However, no DV pH change was seen, indicating that the dominant countercation is some other ion or molecule. Possibilities to investigate in future work include Na^+, K^+, Ca^{2+}, or perhaps positively charged amino acids, and/or other Hb metabolites.

Regardless, since we have also found that PfCRT binds the antimalarial drug CQ (*24*), we were eager to test whether CQ had any affect on the volume perturbations caused by rapid Cl^- withdrawl. Indeed, at meaningful physiologic doses, CQ completely blocked the volume perturbation caused by rapid loss of Cl^- from the DV. This suggests two possible scenarios. (1) PfCRT either forms or regulates a DV Cl^- transport pathway, as suggested previously (*23*), or (2) PfCRT forms or regulates the transport pathway for the companion countercation. Importantly, the relative dose of CQ required to completely block the DV volume decrease in CQR versus CQS strains mirrors the relative dose required for cytotoxicity, suggesting this osmolyte transport function of PfCRT is linked to the mechanism of CQR. This is further supported by the data obtained with the resistance modifier VPL.

We suggest that pH gradient-dependent DV osmolyte traffic differs for CQR versus CQS parasites. Since the rate of Hz production is similar for CQR versus CQS parasites (*9*), which then suggests that the rate of Hb digestion is similar, then CQR parasites are likely not transporting one or more osmolytes out of the DV at the same rate as do CQS parasites. This would explain why the CQR DV is swelled under steady state conditions and why there is a smaller volume change upon ATP depletion. Thus, one or more systems that traffic osmolyte in a pH gradient-dependent fashion are likely partially impaired in CQR parasites; one obvious candidate for this transporter is PfCRT. Additional studies with yeast ISOV expressing various mutant PfCRT isoforms (*23*, *24*) will be helpful in exploring various mechanistic possibilities, as will direct measurements of DV membrane potential versus rapid Cl^- withdrawal.

On the basis of the data in this work and the previous paper, several additional points are important for future work. For example, we suggest that the relationship(s) between drug exposure, inhibition of Hz formation, and DV volume or pH should be quantified. Soluble heme and its associated counterions are also important osmolytes in the DV until the heme is either aggregated or crystallized (in a pH- and drug-dependent fashion). In addition, we note that the DV volume 25 h after infection and before or after glucose starvation differs significantly for CQS versus CQR parasites. This is obviously crucial with regard to comparing drug transport measurements for CQS versus CQR parasites; namely, drug concentrations calculated in many previous studies require further normalization, and certain key conclusions made earlier may be premature. Also, more acidic DV and a larger DV volume predict an even more paradoxical higher level of net accumulation of freely osmotic CQ in CQR DV than previously suggested (*5*). Thus, if the level of net CQ accumulation within the parasite is indeed 2-fold lower at steady state (at a similar dose) for CQR than for CQS, then the mechanism(s) for the decreasing level of net accumulation has an even higher capacity than previously recognized.

Finally, we note an apparent conundrum from the previous paper is resolved via data in this paper. Data from our laboratory and others have previously shown that acidic pH accelerates the rate of Hz formation. Since the DV pH is lower for CQR parasites than for CQS parasites at very early stages of Hz formation, we then expect a faster rate of Hz formation for CQR parasites. Paradoxically, data in the previous paper show that the rate and extent of Hz formation are approximately similar for CQR and CQS parasites.

However, it is also of course true that the rate of Hz formation slows as the noncrystalline heme precursor is diluted. We suggest the increased DV volume (which will dilute the various forms of noncrystalline heme believed to exist in the DV) works to negate pH acceleration of Hz formation such that it is approximately similar for CQS and CQR parasites. At a given CQ concentration, lowering the concentration of soluble heme will act to inhibit drug−heme interaction via simple dilution of the heme target. A lower pH will also do so, and over a wide range of heme concentrations (see refs *8* and *14*), since it will titrate soluble heme into insoluble aggregates that do not readily form complexes with CQ. When the two are put together, the larger volume (diluted heme) and lower pH (less soluble heme) are predicted to be synergistic for heme-targeted antimalarial drug resistance. The degree of synergy observed for any given drug will depend on the relative affinity of that drug for a given form of heme (i.e., monomeric vs μ-oxo dimer vs head-to-tail dimer, all of which likely exist to some level in the DV) as well as the concentrations and pH-dependent solubilities of those forms. Moreover, if we speculate that Hz formation within the DV must proceed at a precise, fixed rate for the parasite to avoid various deleterious consequences, than one altered parameter (e.g., increased DV volume) might represent a fortuitous fitness adaptation in response to an earlier deleterious physiological perturbation (e.g., lower DV pH) that was initially acquired under CQ pressure to confer CQ resistance, but that also then unfortunately acted to accelerate Hz formation in the absence of CQ. Perhaps the different spectra of multiple PfCRT amino acid substitutions, and/or the different combinations of PfMDR and PfCRT alleles found in various CQR strains and isolates, represent different degrees of such fitness adaptation, which then also act to confer variable levels and patterns of observed multidrug resistance. Further calibration of DV pH, volume, and other physiologic parameters in the absence and presence of heme-targeted antimalarials will test these ideas and others.

ACKNOWLEDGMENT

We thank D. Fidock (Albert Einstein College of Medicine, Bronx, NY) for cell lines $C3^{Dd2}$ and $C1^{GC03}$ and Drs. R. Rao (Johns Hopkins University, Baltimore, MD), M. Ferdig (Notre Dame University, Notre Dame, IN), and R. Cooper (Old Dominion University, Norfolk, VA) for helpful discussions.

REFERENCES

1. Robinson, L. J., Roberts, W. K., Ling, T. T., Lamming, D., Sternberg, S. S., and Roepe, P. D. (1997) Human MDR 1 Protein Delays the Apoptotic Cascade in Chinese Hamster Ovary Fibroblasts, *Biochemistry 36*, 11169−78.
2. Huang, Y., Anderle, P., Bussey, K. J., Barbacioru, C., Shankavaram, U., Dai, Z., Reinhold, W. C., Papp, A., Weinstein, J. N., and Sadee, W. (2004) Membrane transporters and channels: Role of the transportome in cancer chemosensitivity and chemoresistance, *Cancer Res. 64* (12), 4294−301.
3. Matsuyama, S., Llopis, J., Deveraux, Q. L., Tsien, R. Y., and Reed, J. C. (2000) Changes in intramitochondrial and cytosolic pH: Early events that modulate caspase activation during apoptosis, *Nat. Cell Biol. 6*, 318−25.
4. Lang, F., Foller, M., Lang, K. S., Lang, P. A., Ritter, M., Gulbins, E., Vereninov, A., and Huber, S. M. (2005) Ion channels in cell proliferation and apoptotic cell death, *J. Membr. Biol. 205* (3), 147−57.
5. Bennett, T. N., Kosar, A. D., Ursos, L. M. B., Dzekunov, S., Sidhu, A. B. S., Fidock, D. A., and Roepe, P. D. (2004) Drug resistance-associated PfCRT mutations confer decreased *Plasmodium falciparum* digestive vacuolar pH, *Mol. Biochem. Parasitol. 133*, 99−114.
6. Leed, A., DuBay, K., Ursos, L. M. B., Sears, D., de Dios, A. C., and Roepe, P. D. (2002) Solution Structures of Antimalarial Drug/Heme Complexes, *Biochemistry 41*, 10245−55.
7. de Dios, A. C., Tycko, R., Ursos, L. M. B., and Roepe, P. D. (2003) NMR Studies of Chloroquine−Ferriprotoporphyrin IX Complex, *J. Phys. Chem. A 107*, 5821−5.
8. Ursos, L. M. B., DuBay, K. F., and Roepe, P. D. (2001) Antimalarial Drugs Influence the pH Dependent Solubility of Heme via Apparent Nucleation Phenomena, *Mol. Biochem. Parasitol. 112*, 11−7.
9. Gligorijevic, B., Ryan McAllister, R., Urbach, J., and Roepe, P. D. (2006) Spinning Disk Confocal Microscopy of Live, Intraerythrocytic Malarial Parasites. 1. Quantification of Hemozoin Development for Drug Sensitive and Resistant Malaria, *Biochemistry 45*, pp 12400-12410.
10. Bray, P. G., Ward, S. A., and O'Neill, P. M. (2005) in *Malaria: Drugs, Disease and Post-Genomic Biology* (Sullivan, D. J., and Krishna, S., Eds.) pp 3−38, Springer-Verlag, Heidelberg, Germany.
11. Goldberg, D. E. (2005) in *Malaria: Drugs, Disease and Post-Genomic Biology* (Sullivan, D. J., and Krishna, S., Eds.) pp 275−92, Springer-Verlag, Heidelberg, Germany.
12. Krogstad, D. J., Schlesinger, P. H., and Gluzman, I. Y. (1985) Antimalarials increase pH in *Plasmodium falciparum*, *J. Cell Biol. 101*, 2302−9.
13. Olson, J. A., and Kilejian, A. (1982) Involvement of spectrin and ATP in infection of resealed erythrocyte ghosts by the human malarial parasite, *Plasmodium falciparum*, *J. Cell Biol. 95*, 757−62.
14. Dzekunov, S., Ursos, L., and Roepe, P. D. (2000) Digestive Vacuolar pH of Intact Intraerythrocytic *P. falciparum* Either Sensitive or Resistant to Chloroquine, *Mol. Biochem. Parasitol. 110*, 107−24.
15. Swedlow, J. R. (2003) Quantitative fluorescence microscopy and image deconvolution, *Methods Cell Biol. 72*, 349−67.
16. Larson, J. M. (2002) 2-D and 3-D deconvolution of confocal fluorescence images by Maximum Likehood Estimation, *Proc. SPIE−Int. Soc. Opt. Eng. 4621*, 86−94.
17. Biggs, D. S. C. (2004) Clearing up deconvolution, *Biophotonics Int. 11* (2), 32−6.
18. Wolf, D. E. (2003) Quantitative digital and video microscopy, *Methods Cell Biol. 72* (15), 319−47.
19. de Monvel, J. B., Le Calvez, S., and Ulfendahl, M. (2001) Image Restoration for Confocal Microscopy: Improving the Limits of Deconvolution, with Application to the Visualization of the Mammalian Hearing Organ, *Biophys. J. 80*, 2455−70.
20. de Monvel, J. B., Scarfone, E., Le Calvez, S., and Ulfendahl, M. (2003) Image-Adaptive Deconvolution for Three-Dimensional Deep Biological Imaging, *Biophys. J. 85*, 3991−4001.
21. Hayward, R., Saliba, K. J., and Kirk, K. (2006) The pH of the Digestive Vacuole of *Plasmodium falciparum* is not Associated with Chloroquine Resistance, *J. Cell Sci. 119*, 1016−25.
22. Martiney, J. A., Ferrer, A. S., Cerami, A., Dzekunov, S., and Roepe, P. D. (1999) Chloroquine Uptake, Altered Partitioning and the Basis of Drug Resistance: Evidence for a Role of Chloride-Dependent Ionic Regulation, in *Transport and Trafficking in the Malaria Infected Erythrocyte*, Novartis Foundation Symposia 226, pp 265−81, Wiley, Winchester, U.K.
23. Zhang, H., Howard, E. M., and Roepe, P. D. (2002) Analysis of the Antimalarial Drug Resistance Protein PfCRT Expressed in Yeast, *J. Biol. Chem. 277*, 49767−75.
24. Zhang, H., Paguio, M., and Roepe, P. D. (2004) The Antimalarial Drug Resistance Protein *Plasmodium falciparum* Chloroquine Resistance Transporter Binds Chloroquine, *Biochemistry 43* (26), 8290−6.
25. Fidock, D. A., Nomura, T., Talley, A. K., Cooper, R. A., Dzekunov, S. D., Ferdig, M. T., Ursos, L. M. B., Su, X.-z., Wooton, J. C., Roepe, P. D., and Wellems, T. E. (2000) Mutations in the Digestive Vacuole Transmembrane Protein PfCRT and Evidence for Their Role in Chloroquine Resistance, *Mol. Cell 6*, 861−71.
26. Sonawane, N. D., Thiagarajah, J. R., and Verkman, A. S. (2002) Chloride concentration in endosomes measured using a ratioable

fluorescent Cl^- indicator: Evidence for chloride accumulation during acidification, *J. Biol. Chem. 277* (7), 5506−13.

27. Busch, G. L., Wiesinger, H., Gulbins, E., Wagner, H. J., Hamprecht, B., and Lang, F. (1996) Effect of astroglial cell swelling on pH of acidic intracellular compartments, *Biochim. Biophys. Acta 1285* (2), 212−8.
28. Mimura, T., Kura-Hotta, M., Tsujimura, T., Ohnishi, M., Miura, M., Okazaki, Y., Mimura, M., Maeshima, M., and Washitani-Nemoto, S. (2003) Rapid increase of vacuolar volume in response to salt stress, *Planta 216* (3), 397−402.
29. Pothos, E. N., Mosharov, E., Liu, K. P., Setlik, W., Haburcak, M., Baldini, G., Gershon, M. D., Tamir, H., and Sulzer, D. (2002) Stimulation-dependent regulation of the pH, volume and quantal size of bovine and rodent secretory vesicles, *J. Physiol. 542* (Part 2), 453−76.
30. Ono, K., Kim, S. O., and Han, J. (2003) Susceptibility of lysosomes to rupture is a determinant for plasma membrane disruption in tumor necrosis factor α-induced cell death, *Mol. Cell. Biol. 23* (2), 665−76.

BI0610348